A 3-D Topographic-Relief-Correlated Monte Carlo Radiative Transfer Simulator for Forest Bidirectional Reflectance Estimation

AUTHOR(S):

Jin, Sheng-Ye; Susaki, Junichi

CITATION:

Jin, Sheng-Ye ...[et al]. A 3-D Topographic-Relief-Correlated Monte Carlo Radiative Transfer Simulator for Forest Bidirectional Reflectance Estimation. IEEE Geoscience and Remote Sensing Letters 2017, 14(6): 964-968

ISSUE DATE:

2017-06-01

URL:

http://hdl.handle.net/2433/229483

A 3-D Topographic Relief Correlated Monte Carlo Radiative Transferring Simulator (TRCMCRTS) for Forest Bidirectional Reflectance Estimation

***Abstract*—Understanding the physical processes that affect electromagnetic waves within forests is a key to a better analysis of global environmental change. In this letter, we propose a 3-D vector model (TRCMCRTS) for estimating a bidirectional reflectance factor (BRF) for a forest with complex terrain relief. Unlike existing models, this model takes into account rugged terrain conditions by modeling ground surface as bilinear surface interpolated from digital elevation model (DEM). The proposed model is compared with the well-performing Monte Carlo model FLiES for validation, and good agreement is obtained. Forest BRF estimations for six different terrain relief conditions are derived, and these BRFs have reasonable variation according to ground conditions.**

***Index Terms*—Monte Carlo Ray-Tracing, Radiative Transferring, Forest, Topographic Relief, Birdirectional Reflectance.**

I. Introduction

The ongoing issue of global environmental change is having a critical impact on the global ecosystem. Understanding of global terrestrial environmental change can be achieved by remote sensing (RS). For example, optical RS helps in mapping vegetated areas and estimating the biological activity of forests. However, optical RS data have been utilized poorly to date in relation to understanding the physical processes of electromagnetic waves in vegetated areas. This situation would be improved with a physical model of the correspondence between optical electromagnetic waves and landscape parameters, which would allow the calibration of optical RS images and the retrieval of landscape parameters. In general, numerical methods based on a radiative transfer equation (RTE) can be used to express the radiative regime. Difficulties in determining the boundary conditions of the radiative transfer (RT) field make solving the RTE problematic [1]. Although Liang and Strahler ingeniously overcame the boundary condition problem by coupling the atmospheric and canopy RTEs, methods for solving RTEs still have innate drawbacks [2]. In particular, properties of the canopy within the RT field are input with average conditions so that individual leaves cannot be distinguished [3], [4].

One approach to accurately estimating the radiation distribution of a complicated landscape is computer simulation, which can be classified into two branches: radiosity modeling [5], [6] and Monte Carlo radiative transfer (MCRT) modeling [7]. For more precise calculations, both radiosity and MCRT modeling methods could be applied to understand the RT field balance and to validate other models. Radiosity modeling aims to render the initialized landscape by means of computer-graphic algorithms. However, despite being able to analyze the input scene from all observation angles, the radiosity method is limited if the landscape complexity exceeds the available computing power. Alternatively, MCRT can provide a faster solution by averaging the RT field at a particular volume scale rather than defining the canopy comprehensively.

When used for solving complicated heterogeneous RT problems, MCRT models provide accurate and robust results and are computationally inexpensive [8]. In MCRT modeling, photon scattering is determined using a phase function rather than by being calculated explicitly as in radiosity modeling. Myneni et al. have summarized the MC models that simulate RT within vegetated areas. They conclude that, apart from the limitations of computational power, MC simulation is an exceptional method that can either trace photon motion within the canopy or determine photon-mass interaction [9]. Disney et al. have comprehensively reviewed subsequent canopy MCRT models [10]. Kobayashi and Iwabuchi developed a three-dimensional (3D) heterogeneous forest RT simulator (FLiES) [11] that was coupled to a one-dimensional (1D) atmospheric RT model by Iwabuchi [12]. This provides remarkable results for flat terrain, but rugged conditions that affect bidirectional reflection in the RT regime make it necessary to include complex topographic reliefs in RT models [13]. In order to consider the RT budget in mountainous areas, a MC approach was developed to solve RTEs for complex ground conditions [14]. This was followed by an RT model that expressed ground relief using a digital elevation model (DEM), thereby addressing the issue of clouds obscuring the observations and also suggesting a way of dealing with complex topographic conditions [15]. More recently, models have been proposed that emphasize the polarization of reflectance by vegetation cover. These assume two types of canopy leaf scattering: Lambertian reflectance and transmittance, or specular reflection [16], [17].

In this letter, we describe a 3D vector MCRT model for estimating the bidirectional reflectance factor (BRF) of a forest area with complicated ground relief. We refer to this model as the Topographic-relief-correlated Monte Carlo Radiative-transfer Simulator (TRCMCRTS). In particular, a solution is developed for retrieving the ground normal vector during ray tracing, which is the key step in determining the scattering direction when a photon hits the ground. In order to evaluate the effects of terrain relief during the simulation, the contribution of single scattering from the ground is estimated. To assess the validity of TRCMCRTS, we compare its estimations of the red and infrared BRFs with those of the FLiES model. Assumed topographic conditions are used to show the extent to which TRCMCRTS is sensitive to different terrain reliefs.

II. Model Delineation

The forest in this model is composed of individual trees distributed heterogeneously in an area with relief topography. In relation to RS observations, the canopy consists of leaves that are particles and branches that are formed as regular geometrical volumes. To take account of topographic effects, the forest scene is divided into a cubic matrix according to the DEM grid of the area. Each cube contains trees and ground objects. Tree objects comprise canopy (leaf), branch (stem), and trunk objects. Ground objects comprise the understory (grass) turbid layer and the soil. The RT simulations are carried out with regard to a reference plane that is higher than the maximum height of the top of the canopy. Only those photons that enter and escape through this reference plane are counted in this model (Fig. 1). In the following, we describe the physical foundations of photon-material interactions in the present context.

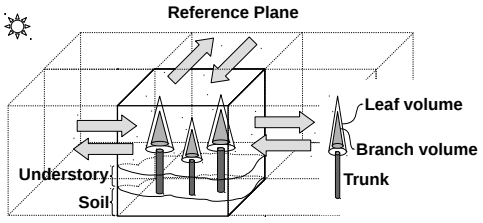

Fig. 1. A sketch of the 3-D scene definition and the components of an individual tree.

A. Topographic Approximation

In the ray-tracing algorithm, a ray is defined mathematically by the parametric line equation

$$\mathbf{r} = \mathbf{r}_0 + t\mathbf{n}_0, \tag{1}$$

where $\mathbf{r}_0 \in \mathbb{R}^3$ is the initial photon position, $\mathbf{n}_0 \in [0,1]^3$ is the directional vector, and t $(t \geq 0)$ is the traveling distance of the photon. The ground is assumed to be a bilinear surface $B(u,v)$ interpolated from the DEM grid:

$$B(u,v) = uv\mathbf{a} + u\mathbf{b} + v\mathbf{c} + \mathbf{d},\ (u,v) \in [0,1]^2, \tag{2}$$

where $\mathbf{a} = \mathbf{p}_{11} - \mathbf{p}_{10} - \mathbf{p}_{01} + \mathbf{p}_{00}$, $\mathbf{b} = \mathbf{p}_{10} - \mathbf{p}_{00}$, $\mathbf{c} = \mathbf{p}_{01} - \mathbf{p}_{00}$, and $\mathbf{d} = \mathbf{p}_{00}$; $\mathbf{p}_{ij}$ for DEM grid point coordinates $\mathbf{p}_{ij}$ with $i,j \in \{0,1\}$. The ray-bilinear intersection algorithm was formed by substituting Eq. (1) into Eq. (2) [18]. The local surface normal $\mathbf{n}_g$ of the ground, which is important for determining the scattering direction of the photon, at the point $\mathbf{p}_g(p_{gx}, p_{gy}, p_{gz})$ is

$$\mathbf{n}_g = \mathbf{n}_x \times \mathbf{n}_y. \tag{3}$$

Here, $\mathbf{n}_x = \mathbf{p}_x - \mathbf{p}_g$ and $\mathbf{n}_y = \mathbf{p}_y - \mathbf{p}_g$, where

$$\begin{aligned} \mathbf{p}_x &= [p_{gx} + \xi, p_{gy}, p_{xz}]^T, \\ \mathbf{p}_y &= [p_{gx}, p_{gy} + \xi, p_{yz}]^T \end{aligned} \tag{4}$$

are two neighboring points of $\mathbf{p}_g$ on $B(u,v)$ in the positive x and y directions, respectively, at a constant distance ξ $(\xi > 0)$. Terms p_{xz} and p_{yz} are the retrieved z coordinates of $\mathbf{p}_x$ and $\mathbf{p}_y$, respectively.

B. Photon trajectories

Photon tracing in the forest scene is implemented within the cubic matrix (Fig. 1). Each cube contains objects such as trees, understory, and soil. The ray-tracing algorithm was designed according to the following scheme:

(i) Initialize new photon.
(ii) Trace photon in cube.
  (a) Determine whether photon interacts with materials (canopy, soil).
  (b) Apply single-leaf or soil scattering.
  (c) Russian roulette to determine whether photon dies.
(iii) Update photon position (Eq. 1).
(iv) If photon passes through reference plane, go to (i).
(v) Else run into next cube and go to (ii).

If the photon dies at step (c), which is determined by the Russian roulette method [11], a new photon is generated. The free path within the canopy is determined by a random number according to Beer's Law. Lambertian scattering is assumed on the material surface. The contribution of photons from the scattering direction to the observation direction is calculated using the local estimation method, and the scattering direction $\Omega_s(\theta_s, \phi_s)$ is determined randomly using the rejection method [19]. The following steps were designed to determine θ_s:

(1) Generate two random numbers ρ_1 and ρ_2 in $(0,1)$.
(2) If $\rho_1 < \rho_2$, go to (1).
(3) Otherwise, $\cos\theta_s = \rho_1,\ \sin\theta_s = \sqrt{1-\rho_1^2}$.

The azimuth ϕ_s is set as follows:

(A) Generate two random numbers ρ_3 and ρ_4 in $(0,1)$.
(B) $f_1 = 1 - 2\rho_3,\ f_2 = 1 - 2\rho_4$.
(C) $\delta = f_1^2 + f_2^2$; if $\delta > 1$, go to (A).
(D) Otherwise, $\cos\phi_s = \frac{f_1}{\sqrt{\delta}},\ \sin\phi_s = \frac{f_2}{\sqrt{\delta}}$.

Therefore, the scattering vector is

$$\mathbf{n}_s = [\sin\theta_s\cos\phi_s, \sin\theta_s\sin\phi_s, \cos\theta_s]^T.$$

Single-leaf scattering is achieved by assuming the leaves to be bi-Lambertian scattering surfaces [20], and the leaf-scattering phase function is created from look-up tables. Lambertian scattering from the soil is achieved by setting the local normal $\mathbf{n}_g$ as the nadir, which means $\mathbf{n}_s$ should be updated by coordinate rotation.

III. Results and Discussion

A. Comparison with FLiES

To validate TRCMCRTS, we compare it with FLiES for a 100 × 100 m^2 area. The 3D scene was defined according to the RAdiation transfer Model Intercomparison (RAMI) Online Model Checker (ROMC) standard [21]. The canopy was formed from spheres whose center height varied from 11.0 m to 19.0 m above ground. Figure 2 shows the comparison between TRCMCRTS and FLiES with 3×10^5 photons for the same input parameters (Table I) in the red (650 nm) and infrared (800 nm) bands with solar zeniths at 20° and 50°.

Figure 2(a-c) shows that the BRF results are highly correlated (correlation coefficients of greater than 0.99) between the two models. The root-mean-square deviations for

TABLE I
PARAMETERS FOR BRF SIMULATIONS

band	450 nm	550 nm	650 nm	800 nm
canopy leaf reflectance	0.038	0.110	0.046	0.050
canopy leaf transmittance	0.017	0.038	0.021	0.045
soil albedo	0.085	0.115	0.15	0.20
solar zenith (°)	20, 50			
leaf area density (m^2/m^3)	2.0			
canopy sphere radius (m)	10			
mean leaf radius (m)	0.1			
leaf angle distribution	spherical			

Fig. 2(a-d) are 0.0014, 0.0012, 0.0086, and 0.0116, respectively. In general, the TRCMCRTS results fit better with the FLiES results under backward-scattering conditions than under forward-scattering conditions; however, the opposite is true in Fig. 2(d). With the same parameter settings for the two MC models, the deviations are mainly due to the particular random-number series that were used. These types of shift could be mitigated crudely by averaging multiple calculation results from TRCMCRTS. However, TRCMCRTS is currently not equipped to remove these variations as this would require further numerical optimization. In order to describe ground reliefs accurately according to the local DEM, TRCMCRTS does not discretize the 3D scene into voxels as does FLiES. Therefore, computational speed is sacrificed at present.

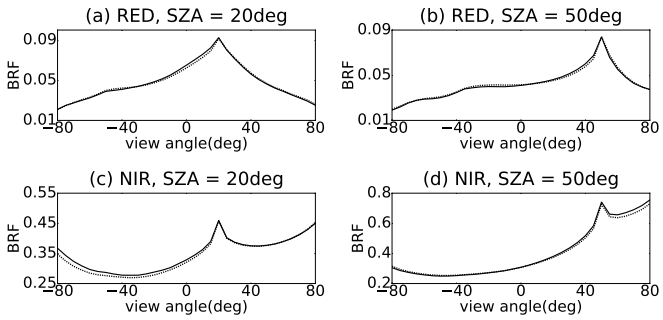

Fig. 2. Comparison simulated BRF results for TRCMCRTS (solid line) and FLiES (dashed line) on the principal plane. Figures (a) and (b) show results for the red band (650 nm) with solar zenith angles (SZAs) of 20° and 50°, respectively; (c) and (d) show the results for the near-infrared band (800 nm) with the same SZAs as (a) and (b), respectively.

B. Topographic Relief

To demonstrate the effect of topography on BRF estimation, six different ground reliefs were assumed (see Fig. 3). In each case, the solar beam was incident from the west ($\theta_0 = 20°$, $\phi_0 = 180°$), and the topographic relief was limited to 0–1.5 m above the ground in order to testify the sensitivity of TRCMCRTS in response to the topography. As shown in Fig. 3, *Condition (a)* is a valley that runs between the top-left and bottom-right corners of the figure. *Condition (b)* is the same as *(a)* but rotated counterclockwise by 90°. Another way to consider the differences between conditions *(a)* and *(b)* is to set *(a)* as the standard. Then condition *(b)* becomes the solar conditions ($\theta_0 = 20°$, $\phi_0 = 90°$), and the observation directions are on a plane that is perpendicular to the observation plane of condition *(a)*. Condition *(c)* is a topography that slopes from the bottom-left to top-right corners of the figure, with two depressions in the top-left and bottom-middle locations. Condition *(d)* is the same as *(c)* but rotated clockwise by 180°. In contrast to the relative azimuth relationship between conditions *(a)* and *(b)*, the solar settings of condition *(c)* are the opposite to those of *(d)*. Condition *(e)* is a ridge that runs between top middle and bottom middle, and is lower on the left than on the right. Condition *(f)* is the same as *(e)* but rotated clockwise by 90°. The relative azimuth relationship between conditions *(e)* and *(f)* is the same as that between conditions *(a)* and *(b)*. The other parameters are given in Table I.

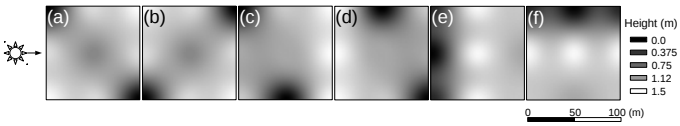

Fig. 3. Different topographic conditions of a 100 × 100 m^2 area used to demonstrate the effect of terrain relief on the BRF. Solar direction is from the west($\theta_0 = 20°$, $\phi_0 = 180°$) in all cases.

First two-row figures of Fig. 4 show the total BRFs of four bands (450, 550, 650, and 800 nm) estimated for the six different topographic conditions shown in Fig. 3. The BRF peak due to the hot-spot effect is the same for all six conditions. The dotted line (g) is for flat ground; all the lines *(a–g)* correspond to the same parameter settings of conditions except the ground conditions. The bottom row figures of Fig. 4 show the single scattering contributions from the canopy. With the same tree parameters (conditions *(a–f)*), the contributions from the canopy are reasonably stable. The contribution from canopy single scattering remains stable for conditions *(a–g)* in each band; hence, the total BRF is affected most by the ground contributions. Compared with condition *(g)* (flat ground), the BRFs from conditions *(a–f)* are enhanced differently. This type of enhancement is found at observation azimuth angles other than just the principal plane (Fig. 5). Conditions *(c)*, *(d)*, and *(f)* show considerable changes in response because of the altered topography.

The correlation coefficient between standard ground (condition *(g)*) and the other conditions of the total BRF can reflect the aforementioned differences between BRF distributions. A lower value of correlation coefficient means that the BRF distribution is affected more by the topography, and vice versa. The values of the correlation coefficient ($\rho_{(g,a)}$) between conditions *(a)* and *(g)* for the four bands are 0.987, 0.989, 0.989, and 0.985, respectively. Comparing conditions (b) and (g), we have $\rho_{(g,b)} = 0.982$, 0.984, 0.980, and 0.983, respectively. Conditions *(a)* and *(b)*, which correspond to a bowl-shaped area located symmetrically around the east-west line, show symmetrical responses at viewing angles around ±60°. Conditions *(c)* and *(d)*, which correspond to symmetrical slopes about the north-south line, present symmetrical responses with variation in observation angle. Condition *(c)* holds obvious phenomenon in comparison with condition *(g)*: we have $\rho_{(g,c)} = 0.961$, 0.971, 0.962, and 0.973, respectively.

The most affected condition is *(d)*: we have $\rho_{(g,d)} = 0.928$, 0.936, 0.924, and 0.971, respectively. Condition *(e)* shows only a small effect because the ground relief has a symmetrical appearance when lit from the front or the back. Condition *(f)*, which is *(e)* rotated clockwise by 90°, produces a strong contribution to the backlit condition: for the four bands, we have $\rho_{(g,e)} = 0.947$, 0.960, 0.949, and 0.972, respectively, and $\rho_{(g,f)} = 0.962$, 0.971, 0.962, and 0.968, respectively. The results for the infrared band (800 nm) are more stable to topographic changes than are the other three bands. In addition, slope conditions *(c)* and *(d)* affect the BRF value more than do the other pairings.

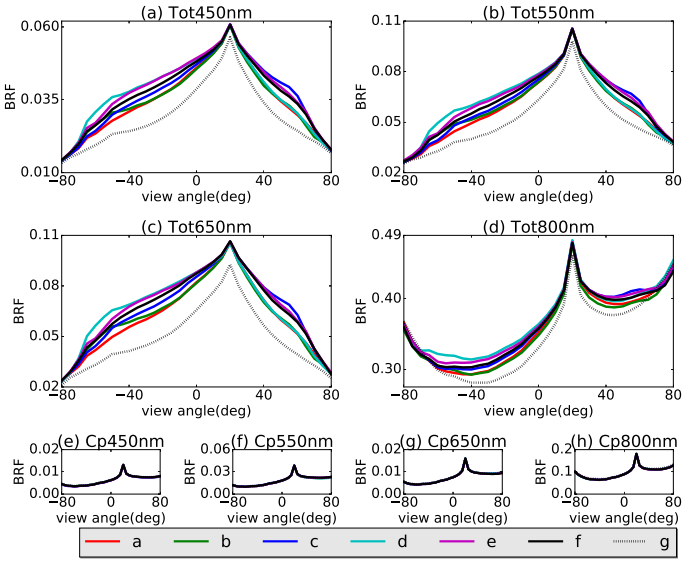

Fig. 4. Total BRF (*(a)-(d)*) of four bands (450, 550, 650 and 800 nm) for the six different topographic conditions (from a to f) in Fig. 3, dot line is with the same parameters but flat ground conditions. Bottom row of figures (*(e)-(h)*) show the canopy single scattering contribution of the four bands.

To assess the topographic effects in detail, Fig. 5 shows the single-scattering contribution from the soil for the six ground conditions and without topography input (condition *(g)*). The model parameters are the same as those for Fig. 4. The topographic conditions enhance the single scattering globally compared with flat ground (condition *(g)*) for azimuth angles of 0–360°. From the results for the four bands, we see growing linear variations from 450 to 800 nm for each ground condition. The BRFs of conditions *(a)* and *(b)* are similar for 450 and 550 nm. The BRF contributions from condition *(b)* are stretched more in the forward-scattering domain at 650 nm compared to condition *(a)*. The contour lines show obvious shifts toward being circular around (45°, 120°) and (45°, 240°). Asymmetrical distributions of BRF are seen for conditions *(c)* and *(d)*. The BRF distributions of the two conditions shows contrary tendencies: the BRF of condition *(c)* is inclined in the 315° direction, whereas that of condition *(d)* tends to 135°. Condition *(d)* also provides a powerful forward-scattering effect. The ridge condition *(e)* supports forward scattering better than does condition *(f)*, which indicates that the angle between the principle plane and the ridge plane also has an impact on the magnitude of the ground scattering. The ridge plane of condition *(e)* is along the middle vertical line perpendicular to the image plane, and that of condition *(f)* is along the middle horizontal line perpendicular to the image plane.

The micro-topographic effect in our model is expressed by estimating the local normal of the point at which light intersects the bilinear surface. This means the scattered photon weight is larger when the relative angle $\Theta_{topography}$ (the angle between the observation direction and the local ground normal) is smaller than Θ_{flat} (the angle between the observation direction and the flare ground normal). According to the Lambertian scattering law, a smaller relative angle gives a higher reflected radiance. This also means that the photon can survive longer after scattering and can contribute more to the BRF estimation.

The ground conditions were selected for the purpose of checking the sensitivity of the model. Hence, the difference between the minimum and maximum elevations is not extreme. Enhancement is shown clearly for ground conditions (c), (d), and (e) . According to the geometry of solar incidence, (c) is stronger for backward scattering and (d) is stronger for forward scattering because (c) and (d) correspond to sloping ground. Condition (c) is also affected by the hot-spot effect, so the enhanced BRF is less obvious than it is for (d). Conditions (a) and (b) show the same symmetrical aspect distribution according to the solar direction, so the enhancements are almost the same. Condition (e) contributes to both forward and backward BRFs because the ridge slopes both forward and backward, whereas (f) shows less enhancement.

Despite the above evidence for systematic enhancement, we cannot conclude that an enhanced BRF estimation would be found for any ground situation. We believe that for some extreme relief conditions like steep hills with a steep gradient on the back side will not be observed. Of course, we must emphasize the important point that the forest must be relatively open so that the reflectance of the bare ground contributes sufficiently to the BRF. The proposed TRCMCRTS contributes micro-topographic effects to the BRF estimation, especially for open forests with bare ground. This type of ground-level local-normal estimation for determining the ground-reflectance contribution accurately can be applied to the local DEM or digital terrain model. Because it calculates the exact interaction between photons and the ground, our model cannot run as fast as can other voxel-optimized models. To accelerate the present model, it may be necessary to implement it in a parallel computing environment.

IV. Conclusion and Future Work

A 3D vector Monte Carlo radiative-transfer model known as TRCMCRTS has been developed to assess the bidirectional reflectance of forests with complex topographic relief. Preliminary results indicate that the model provides similar results for the bidirectional reflectance factor in the red and infrared bands to those of the FLiES model. The present model could be improved by including atmospheric effects in both the physical radiative-transfer modeling of the open forest area and the retrieval of landscape parameters from remotely sensed

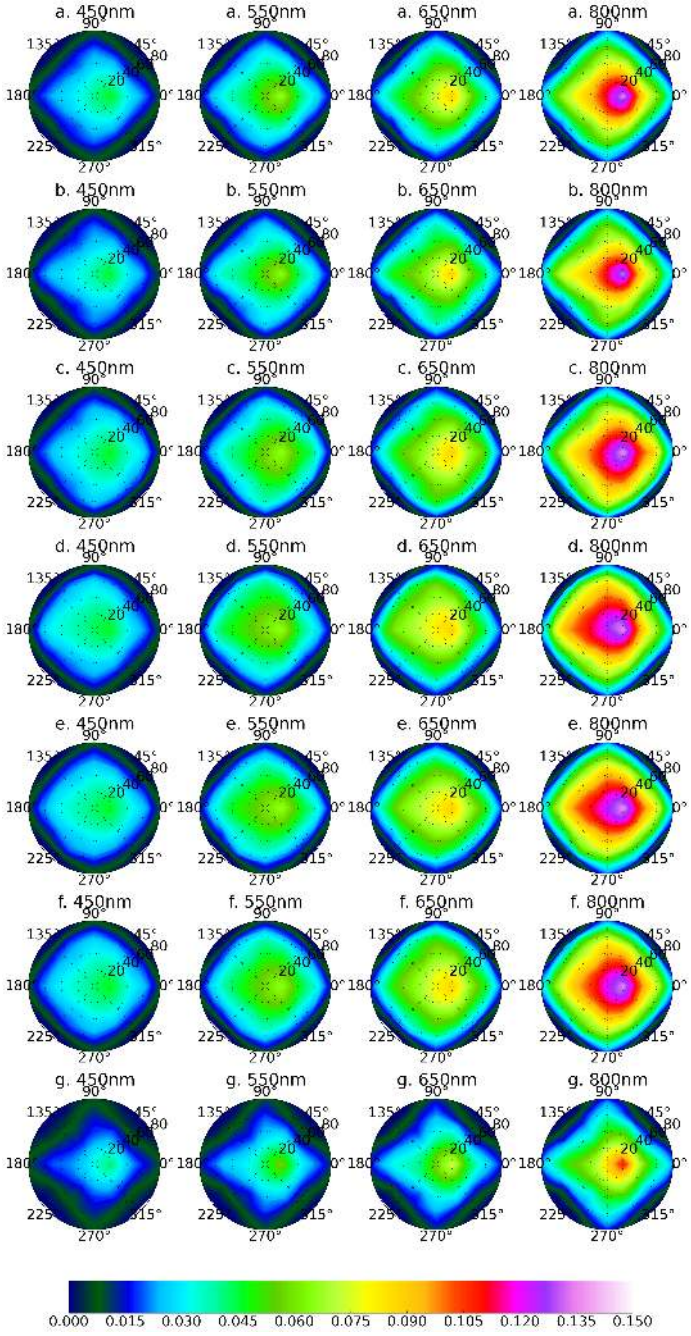

Fig. 5. BRF polar plots of soil single scattering (450, 550, 650, and 800 nm) with Fig. 3 defined topographic conditions from (a) to (f), and flat condition (g). Solar zenith is 20°. Observation zenith varies from 0° to 80°; azimuth are from 0° to 360° with 30° span. Scale bar shows the linear variation from 0.0 to 0.15.

data. However, the present ability to estimate the response according to the topographic relief is more than adequate. Estimations of the ground contribution showed that, for open forest areas, the ground could have an appreciable impact on the BRF distribution, especially if the topographic conditions were considered. Further validation of the TRCMCRTS in the field is planned so that the model can be adjusted to fit with measurements.

ACKNOWLEDGMENT

This research was supported by a program of the Sixth Global Change Observation Mission (GCOM) Research Announcement, Japanese Aerospace Exploration Agency.

REFERENCES

[1] S. Liang, *Quantitative remote sensing of land surfaces*. New Jersey, USA: John Wiley & Sons, 2005, vol. 30.
[2] S. Liang and A. H. Strahler, "An analytic radiative transfer model for a coupled atmosphere and leaf canopy," *Journal of Geophysical Research: Atmospheres*, vol. 100, no. D3, pp. 5085–5094, 1995.
[3] J. P. Gastellu-Etchegorry, F. Zagolski, and J. Romier, "A simple anisotropic reflectance model for homogeneous multilayer canopies," *Remote Sensing of Environment*, vol. 57, no. 1, pp. 22–38, 1996.
[4] B. Ganapol, L. Johnson, C. Hlavka, D. Peterson, and B. Bond, "LCM2: A coupled leaf/canopy radiative transfer model," *Remote Sensing of Environment*, vol. 70, no. 2, pp. 153–166, 11 1999.
[5] C. Borel, S. A. Gerstl, and B. J. Powers, "The radiosity method in optical remote sensing of structured 3-D surfaces," *Remote Sensing of Environment*, vol. 36, no. 1, pp. 13–44, 1991.
[6] N. S. Goel, I. Rozehnal, and R. L. Thompson, "A computer graphics based model for scattering from objects of arbitrary shapes in the optical region," *Remote Sensing of Environment*, vol. 36, no. 2, pp. 73–104, 1991.
[7] P. R. J. North, "Three-dimensional forest light interaction model using a Monte Carlo method," *IEEE Transactions on geoscience and remote sensing*, vol. 34, no. 4, pp. 946–956, 1996.
[8] J. S. Liu, *Monte Carlo strategies in scientific computing*. New York,USA: Springer Science & Business Media, 2008.
[9] R. B. Myneni, J. Ross, and A. G., "A review on the theory of photon transport in leaf canopies," *Agricultural and Forest Meteorology*, vol. 45, pp. 1–153, 1989.
[10] M. I. Disney, P. Lewis, and P. R. J. North, "Monte Carlo ray tracing in optical canopy reflectance modelling," *Remote Sensing Reviews*, vol. 18, no. 2-4, pp. 163–196, 2000.
[11] H. Kobayashi and H. Iwabuchi, "A coupled 1-D atmosphere and 3-D canopy radiative transfer model for canopy reflectance, light environment, and photosynthesis simulation in a heterogeneous landscape," *Remote Sensing of Environment*, vol. 112, no. 1, pp. 173–185, 2008.
[12] H. Iwabuchi, "Efficient Monte Carlo methods for radiative transfer modeling," *Journal of the Atmospheric Sciences*, vol. 63, pp. 2324–2339, 2006.
[13] Y. Chen, A. Hall, and K. N. Liou, "Application of three-dimensional solar radiative transfer to mountains," *Journal of Geophysical Research: Atmospheres*, vol. 111, no. D21, 2006.
[14] C. Miesch, X. Briottet, Y. H. Kerr, and F. Cabot, "Monte Carlo approach for solving the radiative transfer equation over mountainous and heterogeneous areas," *Applied Optics*, vol. 38, no. 36, pp. 7419–7430, 1999.
[15] B. Mayer, "Radiative transfer in the cloudy atmosphere," in *EPJ Web of Conferences*, vol. 1. EDP Sciences, 2009, pp. 75–99.
[16] A. Kallel and J. P. Gastellu-Etchegorry, "3-D vector radiative transfer for vegetation cover polarized BRDF modeling," in *2016 2nd International Conference on Advanced Technologies for Signal and Image Processing (ATSIP)*, March 2016, pp. 499–504.
[17] ——, "Canopy polarized BRDF simulation based on non-stationary Monte Carlo 3-D vector RT modeling ," *Journal of Quantitative Spectroscopy and Radiative Transfer*, vol. 189, pp. 149 – 167, 2017.
[18] S. D. Ramsey, K. Potter, and C. Hansen, "Ray bilinear patch intersections," *Journal of Graphics Tools*, vol. 9, no. 3, pp. 41–47, 2004.
[19] G. I. Marchuk, G. A. Mikhailov, M. A. Nazareliev, R. A. Darbinjan, B. A. Kargin, and B. S. Elepov, *The Monte Carlo methods in atmospheric optics*. Berlin, Germany: Springer, 1980, vol. 12.
[20] J. K. Shultis and R. B. Myneni, "Radiative transfer in vegetation canopies with anisotropic scattering," *Journal of Quantitative Spectroscopy and Radiative Transfer*, vol. 39, no. 2, pp. 115–129, 1988.
[21] J. L. Widlowski, M. Robustelli, M. Disney, J. P. Gastellu-Etchegorry, T. Lavergne, P. Lewis, P. North, B. Pinty, R. Thompson, and M. Verstraete, "The RAMI On-line Model Checker (ROMC): A web-based benchmarking facility for canopy reflectance models," *Remote Sensing of Environment*, vol. 112, no. 3, pp. 1144 – 1150, 2008.